Analysis of a Series of Phenylalanine 57 Mutants of the Adipocyte Lipid-Binding Protein[†]

Melanie A. Simpson and David A. Bernlohr*

Department of Biochemistry, University of Minnesota, St. Paul, Minnesota 55108

Received March 4, 1998; Revised Manuscript Received June 5, 1998

ABSTRACT: The importance of phenylalanine 57, an adipocyte lipid-binding protein (ALBP) portal residue, to ligand affinity and specificity has been investigated using a series of ALBP position 57 mutants. In wild-type ALBP, phenylalanine 57 undergoes a side chain rotation upon ligand binding, moving from an inwardly oriented, ligand-exclusive position in apoprotein structures to an outwardly oriented position in the holoprotein. To examine the role of F57 side chain rotation in the apoprotein−holoprotein transition and in ligand selectivity, ALBP site-specific mutants F57A, F57G, F57H, and F57W were expressed in *Escherichia coli* and purified to homogeneity. Mutants were analyzed for binding characteristics and stability toward chemical denaturation, and energy-minimized models of each mutant were constructed using apo, oleate-, and arachidonate-bound ALBP crystallographic coordinates. The stability of ALBP forms (wtALBP ≈ F57G > F57A > F57W > F57H) was unrelated to the affinity of ALBP forms (wtALBP ≈ F57W > F57H > F57G > F57A) for various lipids and did not vary between fatty acids. Since ligand selectivity was maintained between wild type and all mutants while ligand affinity was grossly diminished, we conclude that phenylalanine 57 is critical to the formation of the fatty acid/ALBP complex, but is uninvolved in determination of selectivity over the range of physiological ligands tested.

The intracellular lipid-binding proteins (iLBPs)[1] are a family of small 15 kDa proteins that bind and sequester a hydrophobic ligand (typically a fatty acid or a retinoid) within a water-filled internal binding cavity. These proteins facilitate the solubilization and delivery of hydrophobic ligands within cells and serve as lipid chaperones, directing the trafficking of such molecules to various locales. Numerous available crystal structures have shown that despite widely varying primary sequence relatedness (20−70%), members of the family are characterized by a superimposable tertiary structure consisting of a flattened 10-stranded β-barrel capped by a helix−turn−helix (*1*, *2*, *3*). The ligand is thought to enter and exit the binding cavity through the helix-capped end of the barrel, and this region is therefore referred to as the portal. Examination of crystal structures reveals higher temperature factors and increased difficulty visualizing electron density of side chain atoms located in this region, which consists of the helices, particularly helix II, and turns between β-strands βC−βD and βE−βF. However, comparison of apo and holo crystal structures is not forthcoming in mechanistic information, since there are no significant changes in most of the structures (*4*−*9*). Furthermore, in most of the crystal structures, there is no visible access from the external milieu to the cavity of sufficient dimensions to accommodate a ligand.

Crystal structures of the adipocyte member of the lipid-binding protein family (ALBP or aP2) in the absence and presence of a bound fatty acid ligand have revealed subtle conformational differences in the region of the portal (*4*). The most significant difference occurs in the position of the side chain of phenylalanine 57, as illustrated in Figure 1. This residue is positioned "downward" over the portal in apo ALBP, but rotates "outward" in all the holo structures. Repositioning allows the β-methylene of F57 to form a van der Waals contact with the ω-methyl of an oleate (*4*), stearate (*4*), or palmitate ligand (*8*), though this contact is not possible for arachidonate because of the O-shaped structure this ligand adopts in the bound crystal form (*9*). Ligand contact is not essential for F57 repositioning, since the alternative conformation is observed for ALBP−arachidonate as well. ALBP forms high-affinity complexes with fatty acids of 14−22 carbons in length, only some of which contact the β-methylene of F57; hence, we reasoned that the interactions between a fatty acid and the side chain of residue F57 could be the basis for ligand selectivity.

To examine the involvement of F57 in ligand-binding affinity and/or selectivity, we generated a series of site-specific mutations at this position. We explored the effect of F57 side chain size and charge upon resistance to chemical denaturation, intrinsic tryptophan fluorescence, binding, and fluorescence characteristics of the fluorescent probe 1-anilinonaphthalene-8-sulfonic acid (1,8-ANS), competition of ANS binding by various fatty acid ligands, and energy-minimized modeling against apo or holo ALBP crystallographic coordinates. Four representative mutants were

[†] This work was supported by NSF Grant MCB 9506088 to D.A.B. and the Minnesota Obesity Center.

* To whom correspondence should be addressed at the Department of Biochemistry, University of Minnesota, St. Paul, MN 55108. E-mail: david-b@biosci.cbs.umn.edu.

[1] Abbreviations: FABP, fatty acid-binding protein; iLBP, intracellular lipid-binding protein; ANS, 1-anilinonaphthalene-8-sulfonic acid; DTNB, 5,5′-dithiobis(2-nitrobenzoate); Gdn-HCl, guanidine hydrochloride; PDB, Brookhaven Protein Database; NMR, nuclear magnetic resonance spectroscopy.

S0006-2960(98)00507-8 CCC: $15.00
Published on Web 07/17/1998

selected: F57G, a mutant in which the side chain has been entirely removed relative to the native residue; F57A, which bears a truncated side chain; F57H, which places a positive charge at the portal; and F57W, which inserts a larger residue. The results of comparison studies between wild-type ALBP and the four mutant forms are presented here with commentary on the significance of residue F57 in ALBP function. Our results demonstrate that F57 in ALBP is critical for modulation of ligand affinity, but is not involved in ligand selectivity.

EXPERIMENTAL PROCEDURES

Materials. Gelase enzyme used in gel purification of restriction enzyme digested PCR fragments was purchased from Epicenter Technologies. All other restriction and DNA modifying enzymes were obtained from Promega. Oligonucleotides used for PCR and DNA sequencing were synthesized by the University of Minnesota Microchemical Facilities. DNA sequencing was performed by the Minnesota Obesity Center (F57H and F57W ALBP) and Microchemical Facilities (F57A and F57G). 1-Anilinonaphthalene-8-sulfonic acid (1,8-ANS) was purchased from Molecular Probes. Fatty acids were from NuChek Prep (Elysian, MN). All other chemicals used were reagent grade obtained from Sigma.

Mutagenesis and Subcloning. Site-specific mutants of ALBP were generated by PCR using internal oligos complementary to a 21-nucleotide sequence encompassing F57. The 5′ 180 nucleotides of the ALBP cDNA were amplified using a 5′ oligo encompassing the ATG start codon in conjunction with the internal F57 oligo. Similarly, the 3′ 210 nucleotides were amplified with the internal F57 oligo and a 3′ external oligo. The 2 resultant fragments were included as templates in a final amplification utilizing the 5′ and 3′ external oligos to regenerate the full-length ALBP cDNA of 400 nucleotides containing the respective substitutions at nucleotides encoding amino acid residue 57. To facilitate subcloning, external oligos for F57H and F57W specified an *Nco*I site at the 5′ end and a 3′ *Bam*HI site. The 5′ *Nco*I restriction site incorporated the ATG start codon, and altered the second amino acid from a cysteine to a glycine as described previously (10). *Nco*I- and *Bam*HI-digested fragments were ligated to the similarly digested expression vector pJMB100A to create plasmids pJMB-F57H and pJMB-F57W. External oligos for F57A and F57G placed an *Nde*I site at the 5′ end and a *Bam*HI site at the 3′ end. In this case, the *Nde*I site also included the ATG start codon, but did not encode an amino acid substitution. The *Nde*−*Bam*-digested fragments were ligated to the pRSETb expression vector, similarly digested, to create plasmids pRSET-F57A and pRSET-F57G. All mutant cDNAs were sequenced to verify the presence of expected mutations and the absence of spurious mutations.

Expression and Purification of Wild-Type ALBP and F57 Mutants. Wild-type ALBP was expressed and purified as previously described (*11*). Briefly, cells are lysed by sonication and cell debris removed by centrifugation at 20000*g* for 30 min. Nucleic acids are precipitated with protamine sulfate and removed by centrifugation at 15000*g* for 20 min. The supernatant is then acidified with sodium acetate (pH 5.0) and allowed to stir at room temperature overnight. The insoluble material is removed by centrifugation and the supernatant concentrated. Following a second centrifugation at 100000*g*, the sample is gel-filtered at neutral pH using a Sephadex G-75 column. ALBP-containing fractions are identified by immunoblotting, concentrated, and dialyzed again. Final purification is accomplished using cation exchange chromatography in sodium acetate, pH 5.2, and eluted with a 0−1 M linear NaCl gradient. Concentrated homogeneous protein is stored in 25 mM Tris-HCl, pH 7.4.

E. coli strain JM101 transformed with plasmids pJMB-F57H and pJMB-F57W was induced to produce the respective ALBP mutant by the addition of 50 μg/mL nalidixic acid, as described for wild-type protein (*11*). F57W ALBP was purified exactly as described for wild-type protein (*10*, *11*). F57H ALBP was found to precipitate during acidification, so the pH 5 acetate precipitation step was omitted from its purification. Rather, the protein was maintained at neutral pH and subjected to anion exchange on a BioRad BioQ column, followed by cation exchange on a BioRad BioS column to achieve a purity of >95%. Plasmids pRSET-F57A and pRSET-F57G were used to transform *E. coli* strain BL21(DE3)pLysS. Protein expression was induced at an OD of 0.8 in 2 × YT medium by the addition of 0.2 mM IPTG, and cells were grown an additional 3 h before harvest by centrifugation and storage at −80 °C. Mutant proteins were purified essentially as described for wild-type protein, with the addition of an anion exchange step at neutral pH prior to cation exchange in pH 5.2 sodium acetate.

Chemical Denaturation and Free Energy of Unfolding. Protein denaturation was monitored by the red-shifting of the intrinsic tryptophan fluorescence emission maxima as previously described (*12*). Briefly, 0.5 μM protein in 25 mM Tris-HCl, pH 7.4, is mixed with increasing concentrations of Gdn-HCl from 0 to 3 M. Fluorescence emission is excited at 285 nm and the spectrum scanned. The emission maximum is plotted as a function of Gdn-HCl concentration to determine C_m (the concentration of denaturant at 50% denaturation), and the Pace method of linear extrapolation (*13*) is then employed to calculate free energies of unfolding. Each value is the result of data compiled from three separate denaturation assays.

Binding Studies. Ligand-binding characteristics of wild-type and mutant ALBP were assessed by use of a fluorophore displacement assay as previously described (*14*). Briefly, each protein was incubated with 1-anilinonaphthalene-8-sulfonic acid, and the emission and excitation maxima of the resulting complexes were determined. The respective excitation and emission maxima were used to measure increases in ANS fluorescence as a function of increasing protein concentration. Binding constants for ANS were determined by Scatchard analysis of the resultant saturation curves. ANS and protein at the dissociation constant values were then preincubated and various ligands used to compete ANS from the binding site. All assays were conducted in 50 mM sodium phosphate buffer (pH 7.4) at 25 °C. Decreasing fluorescence was plotted versus increasing competitor ligand concentration, and curves were fitted to an exponential equation assuming a single set of binding sites to extrapolate the concentration of competitor at half-maximal fluorescence, $[I]_{50}$. Competitor constants for each ligand were then calculated from the equation $K_i = [I]_{50}/(1 + [ANS]_{free}/K_d)$, where K_d is the dissociation constant

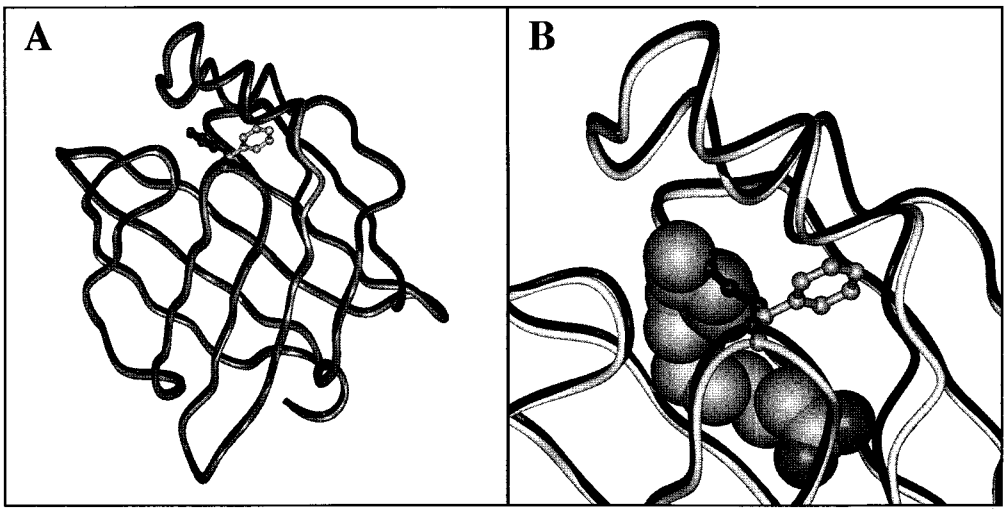

FIGURE 1: Ribbon diagrams of superimposed apo and holo ALBP crystal structures featuring side chain rotation of phenylalanine 57. Ribbons were generated from Brookhaven Protein Database files 1lib (apo ALBP, shown in black) and 1lid (ALBP complexed with oleate, shown in gray). Side chain atoms of residue F57 are depicted by a ball-and-stick rendering. (A) Superimposed apo and holo ALBP structures shown in full view with ligand removed. (B) Enlarged representation of apo and oleate-bound ALBP featuring the portal region and F57 side chain rotation. In this view, the ligand (in dark gray) has been rendered as a space-filling model to demonstrate its contact with residue F57.

determined for the respective wild-type or mutant ALBP/ANS complex.

Energy Minimization. Mutants were modeled against the crystal coordinates for apo ALBP (Brookhaven Protein Database file 1lib) or against ALBP bound to oleate (PDB file 1lid) or arachidonate (PDB file 1adl). Modeling was performed using Insight II 97.0 software (Biosym Inc.), and models were energy-minimized by Discover 3 (included in the Insight II 97.0 suite of programs) under default conditions at pH 7.4. Root-mean-square (rms) deviations were calculated using LSQMAN (*15*), and plotted through O2d (*16*). Plots were overlaid and averaged, and the final figure was constructed in Kaleidagraph.

RESULTS

Phenylalanine 57 is located in the $\beta C-\beta D$ loop, in the region of ALBP known as the portal (Figure 1A). The side chain of this residue is the only ligand-contacting side chain to adopt distinct alternate conformations in the apo vs holo crystal structures (Figure 1B), though the entire region of the protein does exhibit relatively higher temperature factors in both holo and apo forms. To explore the potential impact of this residue on ligand affinity and selectivity, we generated a series of ALBP site-specific mutants in which the F57 side chain was removed (F57G), truncated (F57A), charged (F57H), or enlarged (F57W).

To verify the integrity of each mutant protein structure and assess the relative environment of their respective tryptophan residues, we measured intrinsic tryptophan fluorescence. All ALBP mutants maximally fluoresced at 336 nm when excited at 285 nm, values identical to wild-type protein, suggesting no gross alterations in the tryptophan environment occurred as the result of the amino acid substitution. These values did not vary with the presence of oleate or arachidonate ligands (data not shown), nor did the fluorescence quantum yield change significantly. Furthermore, the molar absorption coefficients were not altered, except in the F57W mutant, in which case the coefficient was increased by approximately 5000 M^{-1} cm^{-1}, as would

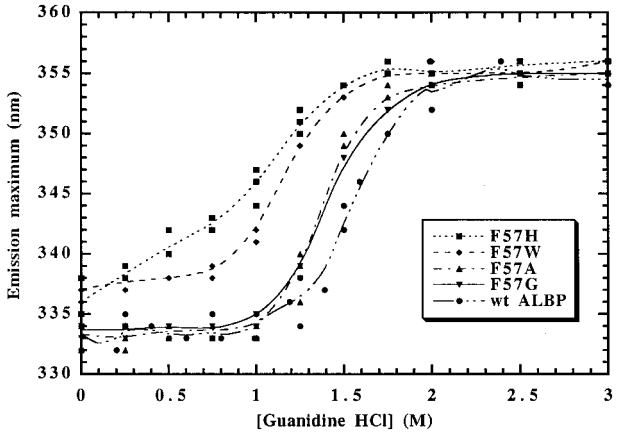

FIGURE 2: Gdn-HCl denaturation effect on the intrinsic tryptophan fluorescence of wild-type and F57 mutant ALBP protein. 0.5 μM ALBP wild-type and F57 mutant protein was incubated with increasing concentrations of Gdn-HCl from 0 to 3 M. Tryptophan fluorescence was excited at 285 nm, and maximum emission wavelengths derived from scanned emission spectra were plotted versus Gdn-HCl concentration. Each curve is a composite drawn through three independently collected data sets. Different symbols denoting the various protein species are as explained in the figure label.

be expected to result from the addition of a tryptophan residue (*17*). The rate of modification of Cys117 by 5,5′-dithiobis(2-nitrobenzoate), DTNB, was not altered between the various mutants and wild type, suggesting structural integrity and similar solvent accessibility to the cavity (data not shown; for reference of technique, see *10*).

Phenylalanine 57 mutants were then evaluated for relative structural stability by resistance to chemical denaturation as measured by the intrinsic tryptophan fluorescence. Increasing concentrations of Gdn-HCl were added to each protein and the excitation and emission properties analyzed. Figure 2 shows the emission maximum plotted against Gdn-HCl concentration. From the progress curves, the C_m (molar concentration of denaturant at 50% denaturation) is obtained, and linear extrapolation through the unfolding transition yields the free energies of unfolding for each protein species

Table 1: Summary of Gdn-HCl Denaturation Characteristics for Wild-Type and F57 Mutant ALBP Forms[a]

	C_m[b] (M Gdn-HCl)	$\Delta G_{unfolding}$[c] (kcal/mol)
ALBP F57	1.55 ± 0.04	5.30 ± 0.29
ALBP F57A	1.40 ± 0.03	4.38 ± 0.23
ALBP F57G	1.42 ± 0.01	5.29 ± 0.30
ALBP F57H	1.05 ± 0.06	1.70 ± 0.24
ALBP F57W	1.18 ± 0.01	3.19 ± 0.26

[a] Gdn-HCl-induced denaturation of F57 ALBP forms was monitored by intrinsic tryptophan fluorescence and used to calculate ΔG, the free energy of unfolding, as described under Experimental Procedures. [b] C_m is defined as the midpoint of the denaturation transition. [c] $\Delta G = -RT \ln K_d$ and represents the free energy of unfolding.

Table 2: 1,8-ANS Binding Properties of Wild-Type and F57 Mutants of ALBP[a]

	excitation λ_{max} (nm)	emission λ_{max} (nm)	K_d (nM)
ALBP F57	370	468	540 ± 50
ALBP F57A	376	474	9000 ± 660
ALBP F57G	376	478	6300 ± 510
ALBP F57H	372	476	2000 ± 570
ALBP F57W	372	472	485 ± 55

[a] Maximum excitation and emission wavelengths for the respective 1,8-ANS/ALBP complexes were determined as described under Experimental Procedures. Binding of 1,8-ANS was measured by the concentration dependence of fluorescence and dissociation constants calculated by fitting to a saturation curve based on a single binding site as described in ref *14*.

(*10*). These values are summarized in Table 1. Wild-type ALBP and the F57G mutant have essentially the same free energies of unfolding, although the C_m for the mutant is somewhat lowered. F57A seems to be slightly less stable to Gdn-HCl than wild-type ALBP, while F57W demonstrates considerably less stability and F57H is most significantly destabilized relative to wild type.

The effect of F57 mutations on the environment in the binding cavity was further addressed using the fluorescent probe 1-anilinonaphthalene-8-sulfonic acid (1,8-ANS). Fluorescence of the probe is negligible in aqueous solvent, but maximal upon sequestration within the binding cavity of the protein. Table 2 summarizes the excitation and emission maxima of ANS complexed with wild-type and mutant ALBP protein species. All of the mutants exhibited red shifts of 4−10 nm in the emission maximum relative to wild-type protein, and, to a lesser extent, similar shifts in the excitation maximum, suggesting some alteration in the fluorophore binding site (e.g., greater solvent accessibility or a more polar environment). The affinities of each mutant and wild-type protein for 1,8-ANS were measured directly by Scatchard analysis of concentration-dependent fluorescence saturation curves. All mutants have significantly decreased affinity relative to wild type except F57W, which exhibits wild-type binding behavior (Table 2). The affinity for 1,8-ANS does not appear to correlate simply with the degree of red-shifting or with the stability of the mutant, since F57G is equally stable but demonstrates more than an order of magnitude decrease in 1,8-ANS-binding affinity whereas F57W is relatively destabilized but demonstrates equivalent 1,8-ANS binding.

To characterize the affinity of each protein for physiological ligands, we utilized the ANS displacement assay previously developed in our laboratory (*14*). In this assay, highly reproducible measurements of the relative ability of a ligand to compete with 1,8-ANS for binding sites are mathematically translated into a displacement or competition constant for that ligand. Figure 3 displays competition curves obtained by addition of increasing concentrations of a variety of fatty acids to preformed 1,8-ANS/ALBP complexes. These fatty acids were chosen to represent high-affinity ligands with a range of properties including shorter chain length (myristate), varying degrees of saturation (oleate, linoleate, and linolenate), and bulkiness (arachidonate, docosahexaenoate). The resultant inhibitor constants, summarized in Table 3, are consistent with those previously published for these fatty acids binding to wild-type ALBP (*18*). With the exception of the affinity of F57W for oleate and linoleate, which is similar to that of wild-type ALBP, competitor constants are higher for the mutants than for wild type by an order of magnitude or more, with all mutants exhibiting the greatest relative affinity for oleate. A comparison of oleate displacement from wild-type and F57 mutant ALBP is illustrated in Figure 4. In order of decreasing affinity, the curves shown are for F57, F57W, F57H, F57G, and F57A. This general trend in relative affinities is observed for each of the ligands assessed in this study. That is, the order of fatty acid affinity among mutants is virtually the same (see Table 4).

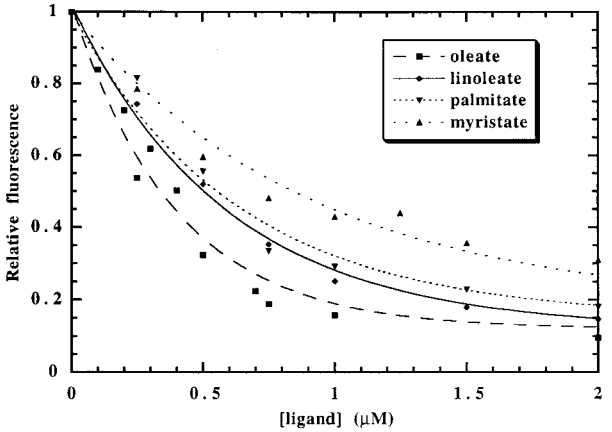

FIGURE 3: Competition of 1,8-ANS binding to wild-type ALBP by various fatty acid ligands. Wild-type ALBP was preincubated with 1,8-ANS and fluorescence measured after successive additions of competitor ligand. Relative fluorescence was plotted as a function of increasing ligand concentration, and the resultant dissociation curves were utilized to determine a K_i. Fatty acid ligands are named in the graph legend in order of greatest to least affinity.

Interestingly, if one calculates the average free energy of fatty acid binding for each ligand, the difference between wild type and each mutant ($\Delta\Delta G$) is very similar: 1.52 ± 0.22 kcal/mol for F57A, 1.28 ± 0.19 kcal/mol for F57G, 0.87 ± 0.41 kcal/mol for F57H, and 0.64 ± 0.35 for F57W. Therefore, the largest change in the free energy of ligand binding between wild type and any mutant form (F57W) is less than 1 kcal/mol whereas the largest difference in the free energy of unfolding between wild type and mutant (F57H) is 3−4 kcal/mol, implying that the energies of unfolding and binding cannot be summed to determine the "true" binding energy for each mutant.

To obtain insights into the structural consequences of F57 substitution, we modeled each mutant against the apo ALBP and oleate- or arachidonate-bound ALBP crystallographic

Table 3: Ligand Affinity and Specificity of ALBP Wild-Type and F57 Mutants Determined by 1,8-ANS Displacement ($K_i \pm$ SD in nM Unless Otherwise Noted)

ligand	ALBP F57	ALBP F57A	ALBP F57G	ALBP F57H	ALBP F57W
myristate 14:0	1320 ± 30	22.6 ± 0.5 μM	13.2 ± 3.1 μM	25 μM	6700 ± 1200
palmitate 16:0	1160 ± 40	≫25 μM	≫25 μM	≫25 μM	5000 ± 1700
oleate 18:1	470 ± 160	331 ± 76	2290 ± 80	1460 ± 220	600 ± 70
linoleate 18:2	534 ± 145	5640 ± 60	3900 ± 100	2700 ± 100	1040 ± 80
linolenate 18:3	553 ± 8	10.8 ± 0.6 μM	5600 ± 200	5300 ± 400	2200 ± 400
arachidonate 20:4	284 ± 21	3380 ± 60	2720 ± 140	ND[a]	ND
DHA 22:6	198 ± 22	3110 ± 10	2380 ± 10	ND	ND

[a] ND = not determined.

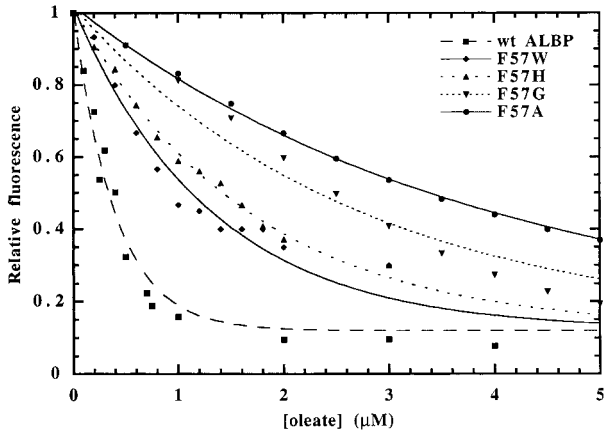

FIGURE 4: Comparison of 1,8-ANS competition by oleate for binding to wild-type and F57 mutant ALBP. Wild-type or mutant ALBP was preincubated with 1,8-ANS and fluorescence measured after additions of oleate competitor ligand. Relative fluorescence was plotted as a function of increasing oleate concentration, and resultant dissociation curves were utilized to determine a K_i.

Table 4: Fatty Acid Selectivity Series among Wild-Type and ALBP F57 Mutants

protein	relative order of affinities
ALBP F57	DHA > Arachidonate > Oleate > Linoleate ≈ Linolenate > Palmitate > Myristate
ALBP F57A	DHA > Arachidonate ≈ Oleate > Linoleate > Linolenate > Myristate > Palmitate
ALBP F57G	DHA ≈ Oleate > Arachidonate > Linoleate > Linolenate > Myristate > Palmitate
ALBP F57H	Oleate > Linoleate > Linolenate > Myristate > Palmitate
ALBP F57W	Oleate > Linoleate > Linolenate > Palmitate > Myristate

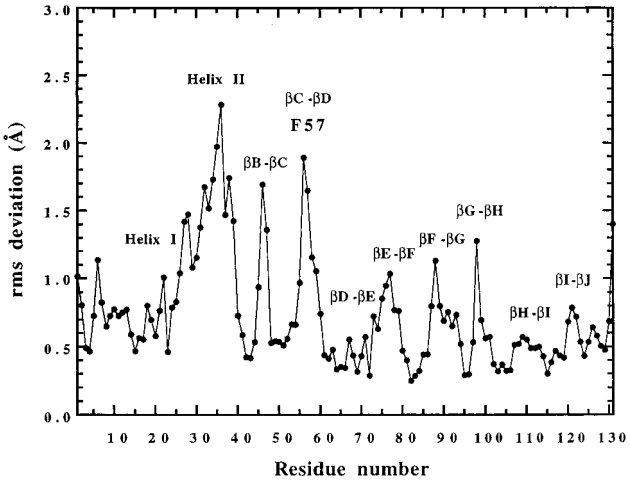

FIGURE 5: Average per-residue root-mean-square deviations for energy-minimized models of wild-type and F57 mutant ALBP. Wild-type apo, oleate-, and arachidonate-bound ALBP crystal structures were energy-minimized using Discover 3 in the Insight II 97.0 suite of programs. F57 mutations were introduced into each of the three crystal structures using Insight II 97.0. The resultant 12 structures were energy-minimized and superimposed, focusing on pairwise comparison of each mutant to its respective wild-type analogue, and each holo model to its relative apo model. Rms deviations for each pair were calculated in LSQMAN, plotted in O2d, and superimposed in Kaleidagraph. The figure presents the average rms deviation for the total superposition, plotted per residue.

coordinates and conducted simple energy minimization on all 3 crystal structures, plus each of the 12 mutant models. Energy-minimized mutant coordinates were superimposed upon the analogous energy-minimized crystal structure coordinates, and rms deviations were calculated and plotted per residue. A composite plot was constructed by averaging and replotting all per-residue rms deviations (Figure 5). The results are consistent with data from intrinsic tryptophan fluorescence which suggested vast differences in protein structure did not occur with energy minimization (pairwise rms deviation ranged from about 0.2 to 2.3 Å) but in all cases the greatest per-residue deviations occurred in the portal region, with α-helix II demonstrating the highest number of energetic minima, followed by the βC−βD loop, α-helix I, the αII−βB loop, and the N-terminal portion of βB. Regions and magnitudes of variability did not appear to correlate with any particular position 57 mutated residue, but rather were innate to the protein conformation itself. This observation is further supported by averaged repeat energy minimizations of wild-type ALBP itself, which superimpose well upon the mutant comprehensive graph shown.

DISCUSSION

Phenylalanine 57 is the only ligand-contacting residue that adopts a significantly different conformation in the unbound vs ligand-bound crystal structure of ALBP. Moreover, in some holo ALBP crystal structures, the ω terminus of the bound lipid is in van der Waals contact with the β-methylene of F57. These observations led to the hypothesis that a primary role for phenylalanine 57 rotation lies in determination of ligand binding selectivity (*2*, *9*). Hence, it was of importance to ascertain via mutational analysis whether alterations at this position would affect the ligand affinity and/or selectivity properties of the protein. The potential involvement of residue F57 in ligand binding by ALBP was studied using a series of site-directed mutants. F57 was mutagenized to glycine to remove the side chain, alanine to truncate the side chain, histidine to charge the side chain, and tryptophan to enlarge the side chain. Additionally, chemical denaturation studies were undertaken to address the issue of correlation between ligand affinity and protein structural stability.

Ligand binding was explored through use of a fluorescence assay developed previously for this purpose. The probe, 1-anilinonaphthalene-8-sulfonic acid (1,8-ANS), fluoresces only when bound within the ligand-binding cavity of the protein. In all cases (Table 2), the excitation and emission maxima were red-shifted, suggesting a probe environment of altered polarity and/or increased access to aqueous quenching effects relative to wild type. For F57W, the hydrophobic character of the amino acid substituted is preserved (*19*), potentially providing an environment of similar polarity for 1,8-ANS to bind. Tryptophan may be able to align similarly to phenylalanine in the 1,8-ANS-bound complex. In the recent crystal structure of ALBP with 1,8-ANS bound as a ligand (*20*), F57 is observed to be in direct van der Waals and/or electrostatic contact with the sulfonate headgroup of 1,8-ANS, which is situated at the fatty acid-binding site in the cavity, but oriented differently. Simultaneously, the sulfonate is complexed with R126, a part of the R106/R126/Y128 fatty acid-binding triad at the base of the cavity. This geometry is accomplished by interaction of F57 with the 1,8-ANS sulfonate moiety, leading to a shifting of the F57 benzene ring and its adherent loop/strands partially into the cavity interior to stabilize the high-affinity complex. Neither alanine nor glycine would have this capacity, which would result in relatively increased polarity/solvent accessibility in the 1,8-ANS-binding site.

In the crystal structure of the V32D/F57H portal mutant previously characterized (*10*), F57H folds back to form a main chain H-bond and no longer projects into the cavity or portal at all. Consistent with the larger opening of the portal region, this mutant form of the protein was found to be 7-fold more rapidly modified by the sulfhydryl-directed reagent dithionitrobenzoate, which rapidly modifies Cys117 in the ALBP-binding cavity. Hence, analogous increased cavity accessibility could occur in the individual F57H mutant, leading to the observed differences in 1,8-ANS binding.

Binding of seven physiological ligands of ALBP was characterized (Table 3). With the exception of F57W binding to oleate and linoleate, the affinities of all mutants for all ligands were dramatically reduced. The array of polyunsaturated ligands bound with affinities an order of magnitude lower than those for wild type, and the saturated ligands failed to show high-affinity binding to any of the mutants. In general, oleate bound all mutants with greatest affinity in the relative order wtALBP $\approx$ F57W > F57H > F57G > F57A. It is possible that contact between the terminal methyl of the ligand and the residue at position 57 may be required for high-affinity binding. This contact is also conserved in intestinal FABP (IFABP): as visualized by NMR, the terminal methyl contacts the βC$-\beta$D and βE$-\beta$F loops. Indeed, prevention of contact by mutagenesis, removing IFABP's helices from the protein entirely, decreased ligand binding 20$-$100-fold (*21*), but global protein stability was also affected by this mutation (*22*). In the case of ALBP, F57/terminal methyl fatty acid contact could occur for oleate, but not for the other ligands. If this contact is highly critical, one would expect wild-type protein to have little affinity for arachidonate and DHA, whose bound conformations render them unable to extend far enough to contact F57 directly, as opposed to the high-affinity binding observed. Maintenance of trends in binding affinity for all mutants and wild-type ALBP to all ligands (see Table 4), coupled with the loss of overall affinity by most mutants, strongly argues for a role of F57 in determining binding affinity, but not specificity (which is conserved in the mutants). Trends in the relative affinity of wild-type ALBP for the ligands discussed in this study are maintained when assayed at 37 °C, as previously published (*18*), additionally arguing for conserved relative enthalpic and entropic contributions to the free energy of binding.

Since affinity could be related to structural stability, that is, the less stable structures would demonstrate lower affinity binding, chemical denaturation studies were conducted to determine free energies of unfolding in the mutants (Table 1). Stabilities from greatest to least were as follows: wtALBP $\approx$ F57G > F57A > F57W > F57H. Wild-type protein is thereby most similar in stability characteristics to the mutants from which it differs most greatly in ligand-binding properties. Hence, it can be concluded that global stability and affinity do not correlate.

To evaluate possible structural changes arising in the mutants, models were generated utilizing both apo ALBP crystal coordinates and those of the oleate- and arachidonate-bound structures. Rms deviations were compared for superimposed energy minimizations of the 3 wild-type apo and holo ALBP structures and the 3 models of each mutant (15 structures in all). The greatest per-residue deviations (Figure 5) occurred in the portal region, and specifically within the α-helices, the βC$-\beta$D loop, the αII$-\beta$B loop, the βE$-\beta$F loop, and the N-terminal portion of βB. Although not correlated specifically with any of our position 57 substitutions, these observations are consistent with the less well-defined electron densities and higher temperature factors reported for these regions by Xu et al. (*4*, *23*), as well as molecular dynamics simulations showing the greatest motion at helix II, the βE$-\beta$F loop (*24*), and, at higher simulated temperatures, the βC$-\beta$D loop (*25*). Furthermore, they are similar to results of energy minimizations of cellular retinol-binding protein, in which helix II and the βC$-\beta$D and βE$-\beta$F loops were most variant (*26*). Modeled, energy-minimized, and crystallographic data demonstrating mobility in these specific protein regions are supported by NMR solution structural data for apo and holo heart FABP (*27*$-$*29*), as well as apo and holo rat intestinal FABP (*30*$-$*32*), human intestinal FABP (*33*), and the ileal lipid-binding protein (*34*), all of which vary most in composite structures at helix II, and the βC$-\beta$D and βE$-\beta$F loops. Helix II in the apo IFABP NMR solution structure is largely disordered in random coil, only developing helical character upon binding of a ligand, at which time it adopts the familiar α-helical structure observed in holo crystals. IFABP's F55 and the remainder of the βC$-\beta$D loop are concurrently pulled toward helix II when it forms. The newly formed structural motifs are stabilized by hydrophobicity, van der Waals contact, and electrostatic interactions (*35*).

Biologically, one potential implication of F57 side chain rotation could be ligand-dependent interaction with other biomolecules. Support for this model derives from studies by Storch and colleagues which examine the transfer of cavity-bound fluorescent fatty acid analogues from FABPs to model membranes (*36*$-$*40*). F57 is located adjacent to a lysine residue analogous to one in heart FABP that was shown to be required for the collisional mediation of ligand transfer to membranes (*36*, *37*). Since ALBP also transfers

its ligands collisionally and with dependence upon surface lysines (*38*, *39*), alteration of F57 orientation could impact the ability of the protein to release ligands. Calculation of individual residue exposure changes upon ligand binding in ALBP shows that rotation of F57 causes a very large increase in exposure of K58, such that its relative change in solvent accessibility is second only to F57 itself (*41*). Gericke et al. (*40*) further demonstrated that ALBP collision during ligand binding and delivery to model membranes actually exerted a transient melting effect on the membrane lipids, and proposed that some small portion of the protein may be partially inserting into the membrane during a delivery collision. The outward flip of F57 may, in fact, serve to provide that insertion point. Interestingly, it was found for heart/muscle FABP that alterations of F57 failed to impact either the ligand affinity or the intrinsic stability of the protein (*42*), whereas both were affected by mutations at position F16. Since HFABP was also found to deliver ligands collisionally, F16 may be fulfilling this role, as the importance of F57 is clearly different for heart/muscle FABP. There are measurable differences between ALBP and heart/muscle FABP at the portal region in all crystal (*4*−*9*) and NMR (*27*−*29*) structures, and structure-based calculations show differences in the topology of the electrostatic surfaces of the proteins (*41*).

The dramatically altered stability and ligand-binding characteristics we have presented for site-specific substitution mutants of ALBP demonstrate that F57 is critical to the bound conformation of the fatty acid/ALBP complex. We conclude that the pivotal role of F57 lies in directing/modulating ligand affinity while ligand specificity is dictated by other elements within the binding cavity. Experiments are underway to determine what aspects of the protein structure determine ligand-binding selectivity.

ACKNOWLEDGMENT

We thank the members of the Bernlohr laboratory, particularly Vince LiCata, for many helpful discussions. In addition, we thank members of the Banaszak laboratory, Joseph Barycki and Jeramia Ory, for their valuable suggestions and critical review of the manuscript.

REFERENCES

1. Banaszak, L., Winter, N., Xu, Z., Bernlohr, D. A., Cowan, S., and Jones, T. A. (1994) *Adv. Protein Chem. 45*, 89−151.
2. Bernlohr, D. A., Simpson, M. A., Hertzel, A. V., and Banaszak, L. J. (1997) *Annu. Rev. Nutr. 17*, 277−303.
3. Veerkamp, J. H., and Maatman, R. G. H. J. (1995) *Prog. Lipid Res. 34*, 17−52.
4. Xu, Z., Bernlohr, D. A., and Banaszak, L. J. (1993) *J. Biol. Chem. 268*, 7874−7884.
5. Sacchettini, J. C., Scapin, G., Gopaul, D., and Gordon, J. I. (1992) *J. Biol. Chem. 267*, 23534−23545.
6. Zanotti, G., Scapin, G., Spadon, P., Veerkamp, J. H., and Sacchettini, J. C. (1992) *J. Biol. Chem. 267*, 18541−18550.
7. Young, A. C. M., Scapin, G., Kromminga, A., Patel, S. B., Veerkamp, J. H., and Sacchettini, J. C. (1994) *Structure 2*, 523−534.
8. LaLonde, J. M., Bernlohr, D. A., and Banaszak, L. J. (1994) *Biochemistry 33*, 4885−4895.
9. LaLonde, J. M., Levenson, M. A., Roe, J. J., Bernlohr, D. A., and Banaszak, L. J. (1994) *J. Biol. Chem. 269*, 25339−25347.
10. Ory, J., Kane, C. D., Simpson, M. A., Banaszak, L. J., and Bernlohr, D. A. (1997) *J. Biol. Chem. 272*, 9793−9801.
11. Xu, Z., Buelt, M. K., Bernlohr, D. A., and Banaszak, L. J. (1991) *J. Biol. Chem. 266*, 14367−14370.
12. Buelt, M. K., Xu, Z., Banaszak, L. J., and Bernlohr, D. A. (1992) *Biochemistry 31*, 3493−3499.
13. Pace, C. N. (1975) *Crit. Rev. Biochem. 3*, 1−43.
14. Kane, C. D., and Bernlohr, D. A. (1996) *Anal. Biochem. 233*, 197−204.
15. Kleywegt, G. J., and Jones, T. A. (1994) *ESF/CCP4 Newslett. 31*, 9−14.
16. Kleywegt, G. J. (1996) *ESF/CCP4 Newslett. 32*, 32−36.
17. van Holde, K. E. (1985) in *Physical Biochemistry*, 2nd edition, p 191, Prentice Hall, Englewood Cliffs, NJ.
18. Simpson, M. A., LiCata, V. J., Ribarik Coe, N., and Bernlohr, D. A. (1997) *Mol. Cell. Biochem.* (in press).
19. Nozaki, Y., and Tanford, C. (1971) *J. Biol. Chem. 246*, 2211−2217.
20. Ory, J., Bratt, J., and Banaszak, L. J. (1998) (manuscript in preparation).
21. Cistola, D. P., Kim, K., Rogl, H., and Frieden, C. (1996) *Biochemistry 35*, 7559−7565.
22. Kim, K., Cistola, D. P., and Frieden, C. (1996) *Biochemistry 35*, 7553−7558.
23. Xu, Z., Bernlohr, D. A., and Banaszak, L. J. (1992) *Biochemistry 31*, 3484−3492.
24. Rich, M. R., and Evans, J. S. (1996) *Biochemistry 35*, 1506−1515.
25. Zanotti, G., Feltre, L., and Spadon, P. (1994) *Biochem. J. 301*, 459−463.
26. van Aalten, D. M. F., Findlay, J. B. C., Amadei, A., and Berendsen, H. J. C. (1995) *Protein Eng. 8*, 1129−1135.
27. Lucke, C., Lassen, D., Kreienkamp, H. J., Spener, F., and Ruterjans, H. (1992) *Eur. J. Biochem. 210*, 901−910.
28. Lassen, D., Lucke, C., Kveder, M., Mesgarzadeh, A., Schmidt, J. M., Specht, B., Lezius, A., Spener, F., and Ruterjans, H. (1995) *Eur. J. Biochem. 230*, 266−280.
29. Lassen, D., Lucke, C., Kromminga, A., Lezius, A., Spener, F., and Ruterjans, H. (1993) *Mol. Cell. Biochem. 123*, 15−22.
30. Hodsdon, M. E., and Cistola, D. P. (1997) *Biochemistry 36(6)*, 1450−1460.
31. Hodsdon, M. E., Ponder, J. W., and Cistola, D. P. (1996) *J. Mol. Biol. 264*, 585−602.
32. Hodsdon, M. E., and Cistola, D. P. (1997) *Biochemistry 36*, 2278−2290.
33. Zhang, F., Lucke, C., Baier, L. J., Sacchettini, J. C., and Hamilton, J. A. (1997) *J. Biomol. NMR 9*, 213−228.
34. Lucke, C., Zhang, F., Ruterjans, H., Hamilton, J. A., and Sacchettini, J. C. (1996) *Structure 4*, 785−800.
35. Sacchettini, J. C., Gordon, J. I., and Banaszak, L. J. (1989) *J. Mol. Biol. 208*, 327−339.
36. Herr, F. M., Aronson, J., and Storch, J. (1996) *Biochemistry 35*, 1296−1303.
37. Wootan, M. G., and Storch, J. (1994) *J. Biol. Chem. 269*, 10517−10523.
38. Wootan, M. G., Bernlohr, D. A., and Storch, J. (1993) *Biochemistry 32*, 8622−8627.
39. Herr, F. M., Matarese, V., Bernlohr, D. A., and Storch, J. (1995) *Biochemistry 34*, 11840−11845.
40. Gericke, A., Smith, E. R., Moore, D. J., Mendelsohn, R., and Storch, J. (1997) *Biochemistry 36*, 8311−8317.
41. Licata, V. J., and Bernlohr, D. A. (1998) (submitted for publication).
42. Prinsen, C. F. M., and Veerkamp, J. H. (1996) *Biochem. J. 314*, 253−260.

BI980507A